Structural inhomogeneities observed in $YBa_2Cu_3O_{7-\delta}$ crystals with optimal transport properties

V. M. Browning, E. F. Skelton, M. S. Osofsky, and S. B. Qadri
Naval Research Laboratory, Washington, DC 20375

J. Z. Hu and L. W. Finger
Geophysical Laboratory and Center for High Pressure Research, Carnegie Institution of Washington, Washington, DC 20015

P. Caubet
Institut National des Sciences Appliquées, Toulouse, France

(Received 19 July 1996; revised manuscript received 24 March 1997)

The high-T_c cuprates have exhibited a variety of unusual features in both their normal-state and superconducting properties. One of the challenges that has faced experimentalists in the field has been to determine whether the observed properties can be attributed to intrinsic behavior or whether they are a result of extrinsic factors such as sample inhomogeneity. In this paper, we present transport measurements on two $YBa_2Cu_3O_{7-\delta}$ crystals which exhibit many of the features generally attributed to fully oxygenated, homogeneous samples. Nevertheless, x-ray-diffraction studies also presented in this paper reveal surface and bulk structural inhomogeneities in both crystals. Results of these studies show variations in the c-axis lattice parameters on the surface and throughout the interiors of both crystals. These are interpreted as variations in the oxygen content. The transport studies together with the structural measurements represent a more thorough and complete characterization of sample quality than is generally reported. Our results lead one to question the validity of using transport measurements alone to determine sample quality and whether any of the properties measured in crystals can be attributed to ''optimally doped'' or ''fully oxygenated'' samples. [S0163-1829(97)01526-9]

I. INTRODUCTION

Despite enormous efforts spent characterizing the transport properties of the high-temperature superconductors (HTS's), the mechanism of superconductivity remains unresolved. Various experimental results including NMR,[1–3] penetration depth,[4] photoemission,[5] and tunneling[6–8] measurements suggest that the charge carriers form superconducting pairs whose wave function exhibits d-wave symmetry as opposed to the s-wave symmetry observed in the conventional low-temperature superconductors. For this reason, numerous new theories which rely on novel pairing mechanisms have been proposed to explain the anomalously high superconducting transition temperatures (T_c) observed in the HTS's. Other theories, such as that of Phillips[9] or Kresin and Wolf,[10] maintain that the HTS's can be understood in terms of conventional phonon-mediated BCS superconductivity, if one takes into account the complexity of the materials' layered structure.

Although the controversy over the origin of superconductivity in the HTS's is still ongoing, considerable progress has been reported in characterizing the transport properties. The determination of the *intrinsic* behavior of the HTS's is crucial. Experimental studies exploring the nature of both vortex dynamics and the mechanism of superconductivity have revealed unusual behaviors which have spawned, or apparently confirmed, some exotic theories. Many of the more well-studied transport properties have generally been accepted as representative of intrinsic behavior, based upon the quality of the samples under consideration. The determination of sample quality is in turn generally based upon the transport properties rather than on any structural examinations, despite the results of several studies which have suggested the presence of inhomogeneities in polycrystalline samples,[11] crystals,[12–18] and films[19] of $YBa_2Cu_3O_{7-\delta}$ (YBCO).

A low resistivity, high T_c, and sharp superconducting transition are generally associated with high-quality samples.[20,21] In terms of these criteria, single crystals are considered better quality than thin-film or polycrystalline samples. For this reason many experiments have focused on high-quality single-crystal samples; they are presumed most likely to be defect free and representative of the intrinsic nature of the materials. Recent results reported by Qadri *et al.*[22] suggest that this may not be true. Using high-resolution x-ray-diffraction studies, they have shown that structural defects exist even in samples with high, sharp superconducting transitions. Assuming that random oxygen defects affect normal-state transport in the Cu-O planes through scattering, the mean free path in the a-b plane must be related to the density of these defects. The average distance between defects is approximately $a/\sqrt{\delta}$. Using $a = 3.8$ Å, this approximation yields an average separation of 15 Å for a $\delta = 0.06$. The interpretation of normal-state properties must, therefore, consider the effects of scattering with mean free paths on the order of tens of angstroms, even in nearly optimally doped samples.

In addition to the transport properties already mentioned, single-crystal samples of HTS's (in particular the 123 cuprates) have exhibited a variety of unusual features in both the normal and mixed states. The normal-state properties include a linear temperature dependent resistivity[23] as well as a temperature-dependent Hall coefficient.[20,24–26] The mixed-

state properties include a sharp drop in the temperature dependence of the magnetoresistivity[27–30] which is attributed to a vortex lattice ''melting'' transition and a negative Hall anomaly[31–34] which occurs in a range of fields and temperatures near T_c. The observation of these features also has been attributed to intrinsic effects based on the ''high quality'' of the crystals. The superconductive properties are expected to be sensitive to sample inhomogeneities due to the short superconducting coherence lengths of these materials, their chemical complexity, their low carrier concentrations, and the strong dependence of their carrier concentrations on the oxygen content. Phillips[9] has shown theoretically that such sample inhomogeneities can explain many of the properties of these systems and has suggested that they are responsible for the high T_c's. At issue is whether defects do indeed exist in samples which have been determined to be high quality (i.e., optimally doped and homogeneous) based on transport measurements alone. If so, then the interpretation of any results obtained on these samples must take into account the presence of these defects or explain why they are irrelevant.

As is well known, the superconducting properties of YBCO are strongly affected by the oxygen composition and ordering in the CuO-basal planes. In general, superconductivity occurs for $7-\delta > 6.4$, with T_c increasing to 93 K for $7-\delta \approx 6.95$ and then decreasing slightly as $7-\delta$ increases to 7.0.[35,36] Under certain processing conditions,[37–44] the curve of T_c versus $7-\delta$ has several plateaus, one near $7-\delta = 7.0$ corresponding to $T_c \approx 90$ K (the ortho-I phase) and others with lower T_c's. The most studied of these is the one near $7-\delta = 6.5$ with a T_c of 60 K (the ortho-II phase). These different T_c's, which can be quite sharp, have been explained as due to the ordering of the chain oxygens. This argument is supported by x-ray-, neutron-, and electron-diffraction measurements.[45–47]

If the chains are not ordered, then T_c still decreases as $7-\delta$ decreases, but the transitions tend to broaden and no T_c plateaus are observed.[48] Parks *et al.*[49] have shown that the c-axis lattice parameter of the orthorhombic unit cell is a reliable measure of the oxygen composition for bulk samples with disordered oxygen chains. Skelton *et al.*,[50,51] using energy-dispersive x-ray-diffraction techniques with synchrotron radiation, studied the variation of the c-lattice parameter of single crystals of YBCO with a spatial resolution of 50 μm^2. In one case, it was found that while the c-lattice parameter remained invariant in the central region of the crystal, it increased towards the surfaces, which could be interpreted as evidence that the oxygen content diminishes near the sample surfaces. In a recent Letter, Qadri *et al.* reported the detection of variations in the c-axis lattice parameter near the surfaces of YBCO crystals based on high-resolution x-ray-diffraction studies.[22]

The work reported in this paper represents a continuation of earlier efforts. In an effort to determine whether defects may exist in samples which exhibit many of the criteria generally attributed to ''high-quality'' crystals, we have performed a series of transport measurements on two single-crystal samples. These crystals were further analyzed using high-resolution x-ray-diffraction studies to examine the crystals' surface and very-high-energy x-ray photons to probe the crystals' interior. The transport measurements coupled with the structural studies represent the most thorough characterization of HTS samples reported to date. The results have striking implications for current theories and indicate that despite exhibiting all of the transport properties that are generally associated with high-quality crystals, our samples contain oxygen defects. This brings into question the assumption that samples can be determined to be optimally doped, homogeneous crystals based on transport properties alone. Unless these oxygen content assumptions can be verified independently, e.g., via structural studies, claims that experimental results are intrinsic, especially below T_c, are suspect.

II. TRANSPORT MEASUREMENTS

The crystals were grown in a zirconia crucible using a self-decanting flux method.[52] Crystals grown using this method are generally heavily twinned and both samples were determined by visual inspection with polarized light to be equally twinned along both crystallographic directions. Electrical contacts were made by sputtering 200 nm gold stripes along the edges of the crystal to which 25-μm diameter gold wires were attached using silver epoxy. A high-temperature anneal in flowing oxygen was applied to reduce the contact resistances to less than 1 Ω at room temperature.

Magnetotransport measurements were taken in a 13-T superconducting magnet. The sample was oriented in field using a Hall sensor placed adjacent to the sample which in turn was mounted on a goniometer that allowed sample rotation in field. Hall effect measurements were performed with the magnetic field oriented along the c axis by either sweeping the field with the sample held at fixed temperature or by sweeping the temperature with the sample held at fixed field. Measurements were made using both positive and negative fields in order to correct for magnetoresistance due to small misalignments of voltage contacts.

Low contact resistances do not necessarily imply a uniform contact over the entire contact area. Nonuniform contacts could result in an inhomogeneous current distribution which might compromise the experimental results. In order to verify a uniform current distribution, measurements were made using various sets of voltage contacts. Voltage was measured using several pairs of contacts, and the degree to which resistivity measurements agree among the various combinations of voltage contacts was taken as a measure of the current uniformity. In both samples, it was determined that the current distribution was highly uniform. In order to rule out sample heating effects, I-V curves were taken above T_c and determined to be Ohmic within the range of the applied measuring currents (10–20 mA).

A. Resistivity

Figure 1 shows the resistivity versus temperature data obtained from the two crystals. Both samples exhibited a high (>93 K) and sharp (<300 mK) superconducting transition. In addition, the resistivity at $T=300$ K and the residual resistivity are both within the range of resistivities reported for high-quality twinned samples. As mentioned previously, a linear temperature-dependent resistivity is also generally considered a criteria for judging sample quality. Halbritter[16] has proposed a model which relates the slope α and zero-

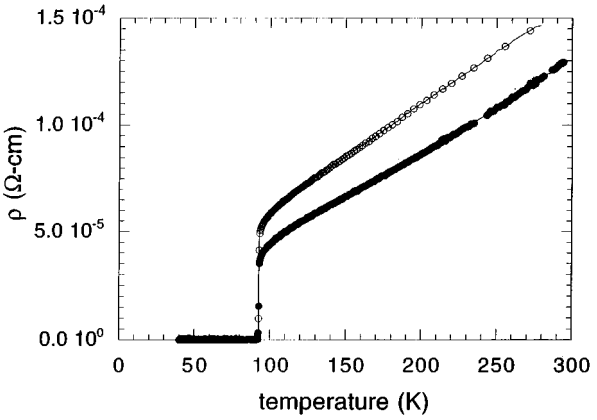

FIG. 1. Resistivity vs temperature for single-crystal $YBa_2Cu_3O_{7-\delta}$ sample A (solid circles) and sample B (open circle).

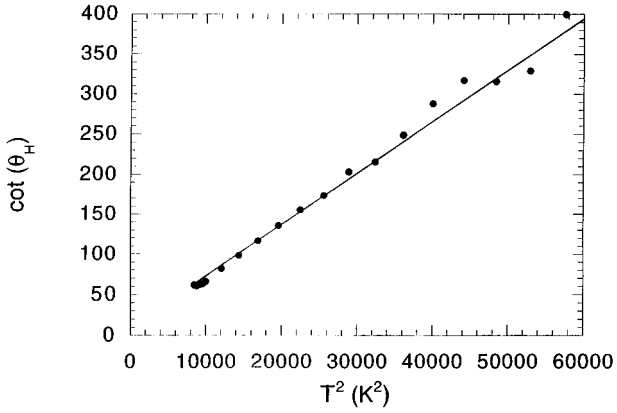

FIG. 2. Temperature dependence of $\cot(\theta_H)$ as measured in a single-crystal sample of $YBa_2Cu_3O_{7-\delta}$ (sample A). The solid line represents a fit of a T^2 temperature dependence to the data.

temperature intercept $\rho(0)$ to sample inhomogeneities. Both samples exhibited a highly linear temperature dependence with $\rho(0)=14.5\ (-6.0)\ \mu\Omega$ cm and $\alpha=0.5\ (0.5)$ $\mu\Omega$ cm/K for sample A (B). These results are in agreement with the reported intrinsic values as determined from measurements obtained from fully oxygenated thin film samples.[53]

B. Normal-state Hall effect

The observed $1/T$ temperature dependence of the Hall resistivity (ρ_{xy}) together with the linear dependence of the normal-state resistivity (ρ_{xx}) has provided considerable evidence which suggests that the temperature dependence of $\cot(\theta_H)\equiv\rho_{xx}/\rho_{xy}$ obeys a strict T^2 dependence.[54,55] Several models have been proposed to account for these observations. Anderson[56] suggests that the observed temperature dependence is due to different relaxation rates for charge and spin carriers. Carrington *et al.*[57] propose that the observed temperature dependences can be explained in terms of variations of the mean free path around the Fermi surface, while other models suggest that the temperature dependence reflects an actual change in carrier concentration.[58,59] All of the above-mentioned models assume that the observed T^2 dependence of $\cot(\theta_H)$ is intrinsic in nature based on the high quality of their samples as determined by low resistivities, high T_c, and/or conventional x-ray-diffraction techniques. For comparison, our $\cot(\theta_H)$ values for sample A as calculated from our resistivity and Hall measurements are plotted in Fig. 2. Similar results (not shown) were obtained for sample B. The solid line represents a fit of the equation aT^2+b to the data. The coefficients $a=0.006$ and $b=10$ obtained from this fit are found to be in agreement with those of Chien *et al.*[32]

As already mentioned, due to the short coherence length in the a-b plane ($\xi_{ab}\sim 20-30$ Å), the superconducting order parameter is also highly sensitive to structural inhomogeneities on similar length scales. We shall now discuss several features of the superconducting state which are generally attributed to intrinsic effects and which are often observed in only the highest-quality samples.

C. Negative Hall anomaly

Rice *et al.*[60] have measured the Hall effect in a detwinned single-crystal YBCO sample below T_c. The crystal measured in their study exhibited a very high, sharp superconducting transition and resistivity values that were among the lowest ever reported. Their results are consistent with similar measurements in twinned YBCO films[61,62] and crystals[63] and in $Bi_2Sr_2CaCu_2O_{8+y}$ and $Tl_2Ba_2CaCu_2O_8$ films[64,65] in that the Hall resistivity undergoes a sign change in a range of magnetic fields and temperatures below T_c. Their results are interpreted in light of a model presented by Wang and Ting[66] which relies heavily on pinning forces. It is argued that although their results are well described by the Wang-Ting model, the fact that a similar negative Hall anomaly is seen in thin-film samples suggests that this model is not appropriate since the pinning forces would be expected to be quite different. Although additional pinning forces are expected in thin films due to grain boundaries, it could be argued that since the effect is seen in single crystals, the relevant pinning forces originate within the grains and that the lack of discrepancy between thin-film and crystal samples is, therefore, not surprising.

Harris *et al.*[63] have studied the angular dependence of the negative Hall anomaly and originally argued that the observed sign change in ρ_{xy} arose due to fluctuations associated with a Magnus force that changes sign depending on whether vortices are aligned in plane or out of plane. However, in light of new evidence[67] which suggests that the Hall conductivity (σ_{xy}) scales with the angle between the c axis and the applied field, Harris *et al.* now argue that the negative Hall anomaly can be better understood in terms of a model proposed by Geshkenbein and Larkin.[68] In this model, the sign change arises in a two-component system[69] in which the quasiparticle and vortex Hall currents have opposite sign. Harris *et al.* demonstrated the expected scaling of σ_{xy} with respect to field and tilt angle which has provided strong evidence in support of the Geshkenbein-Larkin model. Implicit in the interpretation of the results of both Harris *et al.* and Rice *et al.* is the assumption (based upon low resistivity values and high, sharp superconducting transitions) of highly oxygenated, homogeneous samples.

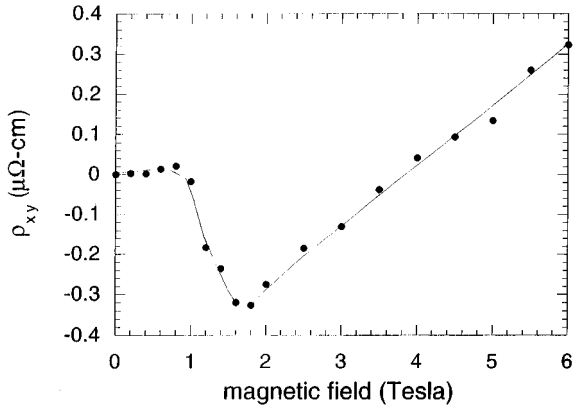

FIG. 3. Field dependence of ρ_{xy} below T_c for single-crystal $YBa_2Cu_3O_{7-\delta}$ (sample A). The solid line is a guide to the eye.

The negative Hall anomaly observed in sample A at a temperature of 89.9 K is plotted in Fig. 3. The depth of the resistive minimum is consistent with that obtained by Rice *et al.*; however, we also observed an angular dependence similar to that of Harris *et al.* The fact that our structural studies show evidence of sample inhomogeneity suggests that models such as that of Wang and Ting, which incorporate pinning forces due to sample defects, may be appropriate for describing the negative Hall anomaly.

D. Magnetoresistance

A sharp resistive drop in the mixed state of ''clean'' single-crystal YBCO samples in the presence of applied magnetic fields has been interpreted as evidence for a vortex lattice melting transition.[70,71] This drop occurs at a resistivity value that is approximately 10% of the normal state resistivity and is $\sim 100-200$ mK wide in low fields. It was further shown by Kwok *et al.*[71] that this effect could be suppressed by pinning at twin boundaries. This observation was interpreted as evidence that the effect is intrinsic and that an increase of pinning sites due to the presence of various sample defects would further suppress the effect. For this reason, the observation of this melting transition is taken to be a signature of high-quality samples.

Our magnetoresistance results for sample A are shown in Fig. 4. The inset shows similar data for sample B taken in an applied field of 4 T. The angular dependence of the magnetoresistance is shown in Fig. 5 and suggests, in agreement with the results of Kwok's *et al.*, that pinning at twin boundaries suppresses the effect. However, the results of our structural studies, which we will now discuss, indicate the presence of various oxygen defects which preclude ruling out the possibility that this effect is extrinsic in nature.

III. STRUCTURAL STUDIES

A. High-resolution surface measurements

High-resolution x-ray-diffraction measurements were performed on a Huber four-circle diffractometer using triple-crystal arrangement in which the monochromating and the analyzing crystals were both Ge(111) (see Fig. 6). Cu $K\alpha$ radiation from a rotating-anode x-ray tube was used. The

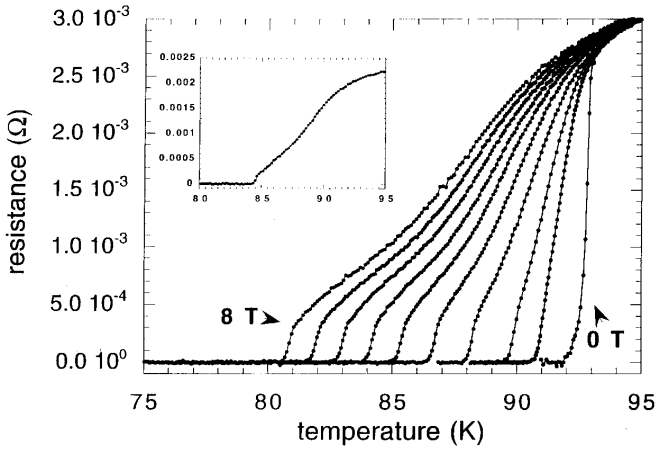

FIG. 4. Magnetoresistance vs temperature for single-crystal $YBa_2Cu_3O_{7-\delta}$ (sample A) as a function of applied field. The field was applied at an angle of 30° with respect to the crystal's c axis in order to avoid pinning at twin boundaries. Data are shown for $H = 0$, 0.5, 1, 2, 3, 4, 5, 6, 7, and 8 T. The inset shows similar data obtained from sample B in an applied field of 4 T.

$K\alpha_2$ peak was eliminated by adjusting the aperture slits between the monochromating crystal and the sample. The absorption length ($1/\mu$, where μ is the linear absorption coefficient) for Cu $K\alpha$ radiation in YBCO is 9.1 μm. The reciprocal of the attenuation coefficient for the (006) reflections, also for Cu $K\alpha$ radiation, is 1.7 μm.[72] These values bracket the upper and lower absorption limits between mosaic and perfect crystals. They are representative of the depth of material being sampled in these high resolution measurements.

Scans along the $[0,0,l]$ reciprocal lattice vector, i.e., so-called θ-2θ scans, of the (0,0,6) reflection are shown in Fig. 1 for each crystal. Each scan can be resolved into three separate peaks, each corresponding to a slightly different c-axis

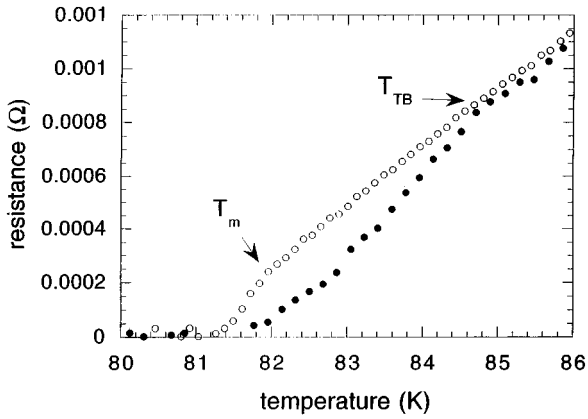

FIG. 5. Angular dependence of the magnetoresistance showing suppression of the ''melting'' transition due to pinning at twin boundaries. The two curves represent data taken in an applied field of 8 T with $\theta = 0°$ (solid circles) and $\theta = 16°$ (open circles) where θ is defined as the angle between the crystal's c axis and the applied field.

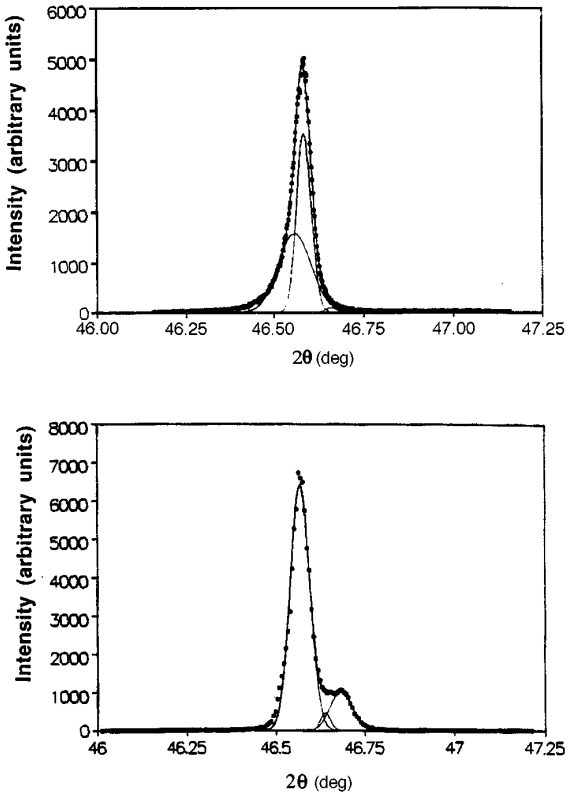

FIG. 6. High-resolution specula scan of the (006) reflection for samples A (bottom) and B (top) taken on triple-crystal diffractometer with Cu $K\alpha_1$ radiation. In this configuration, the Cu $K\alpha_2$ component was eliminated by adjusting the slits after the monochromator. The monochromator and analyzing crystals were Ge (111).

parameter. When examined using a conventional single-crystal diffractometer with a graphite analyzer, only a single broad peak is seen. The angular resolution of our conventional diffractometer is about 7 arc minutes, whereas that of our high-resolution diffractometer is about 9 arc seconds.

The c-axis lattice parameter of the YBCO orthorhombic unit cell is a reliable indicator of the oxygen content in crystals. It is related to oxygen composition by the equation

$$7-\delta=74.49-5.787c, \tag{1}$$

where c is in angstroms.[52] (This equation does not hold for YBCO thin films.) The estimated uncertainty in δ is ± 0.04. Based on this equation, the values of $(7-\delta)$, as determined from the high-resolution scans, are given in Table I. The integrated area under each peak is representative of the fraction of the illuminated area associated with the oxygen content corresponding to that peak. These values also are given in Table I. It is important to note that in these crystals, as in most every YBCO crystal we have studied, there is always a region with $(7-\delta)\sim 7.0$. The fact that we never obtain regions with $(7-\delta)>7.0$, within the experimental uncertainty, gives us confidence in the validity of Eq. (1) for determining the oxygen content. The weighted average of $(7-\delta)$ for each crystal is the same: 6.87 ± 0.04 for crystal A and 6.84 ± 0.04 for crystal B.

To obtain information about the quality of individual grains or domains, rocking curves were measured. The (006) reflection of each crystal was centered in ω and χ with 2θ set at 46.40°. The measured rocking curves are shown in Fig. 7. For crystal A the measured peak can be deconvoluted into seven separate peaks; crystal B can be represented by five peaks. These multiple peaks may be due to different oxygen concentrations and small-angle grain boundaries between crystallites.

B. High-energy bulk measurements

In order to probe the interior of these crystals, the very-high-energy x rays available at the National Synchrotron Light Source (NSLS), at Brookhaven National Laboratory were used. The energy dispersive diffraction facility on Beamline X17C at NSLS, which was used for this work, has been described elsewhere.[73] Complete details of the standard techniques used to analyze the energy-dispersive x-ray-diffraction data can be found in Ref. 50.

1. Data collection

The cross section (width and height) of the beam impinging on the sample is defined by four tungsten blocks. These are controlled by computer-driven micropositioners and were set to define a beam approximately 10 μm wide and 10 μm high. The actual cross section was determined by stepping a knife edge through the beam at 1-μm intervals and monitoring the transmitted intensity I_0. The full width at half maxi-

TABLE I. Peak intensities, 2θ values, c-axis lattice parameters, and $7-\delta$ values as obtained from high-resolution 2θ scans of $YBa_2Cu_3O_{7-\delta}$ crystals A and B shown in Figs. 9(a) and 9(b), respectively.

Crystal A Peak position (2θ)	Relative intensity	Surface area (%)	c (Å)	$7-\delta$
46.546	288	37.5	11.6965	6.82
46.586	456	59.3	11.6868	6.86
46.685	24	3.2	11.6633	6.99
Crystal B Peak position (2θ)	Relative intensity	Surface area(%)	c (Å)	$7-\delta$
46.569	439	82.0	11.6097	6.84
46.639	16	3.1	11.6741	6.93
46.683	79	14.9	11.6637	6.99

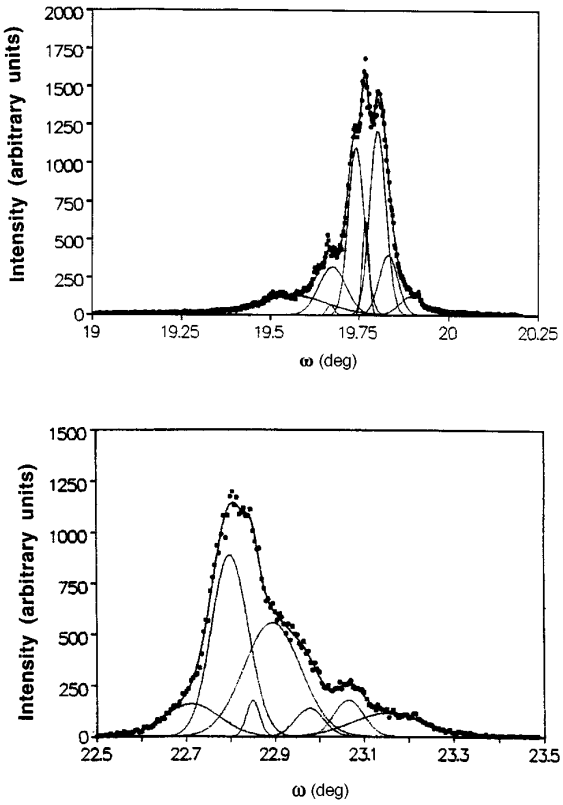

FIG. 7. The rocking curve of the (006) diffraction peak for the sample taken with Cu $K\alpha_1$ radiation for samples A (bottom) and B (top).

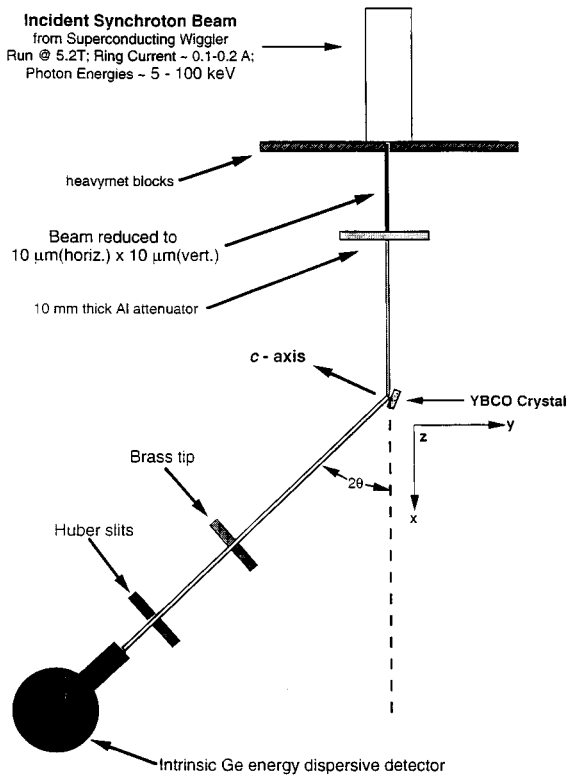

FIG. 8. Schematic of the high-energy diffraction experimental set up on Beamline X17C at NSLS.

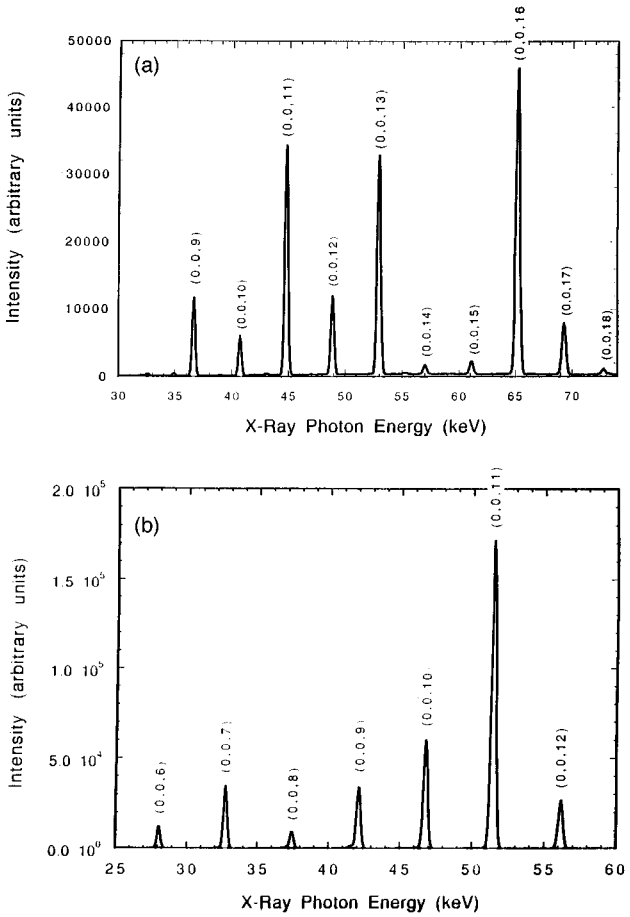

FIG. 9. (a) $(0,0,l)$ diffraction spectrum for $YBa_2Cu_3O_{7-\delta}$ crystal A recorded at $2\theta = 15.000°$. (b) $(0,0,l)$ diffraction spectrum for $YBa_2Cu_3O_{7-\delta}$ crystal B recorded at $2\theta = 13.000°$.

mum of plots of dI_0/dy versus y and of dI_0/dz versus z were used to determined the actual width and height, respectively. These values were 19.2 and 9.4 μm, respectively, for crystal A and 10.5 and 9.0 μm, respectively, for crystal B.

Each crystal was bonded to a glass fiber and mounted on a four-circle $(2\theta,\omega,\chi,\phi)$ diffractometer with its $[0,0,l]$ reciprocal lattice vector approximately in the horizontal plane at $\chi \approx 0$ and normal to the incident beam at $\omega \approx 0$. (The angle ϕ was held constant during these experiments.) The crystal was then approximately centered in the beam optically. With $\omega \approx \chi \approx 0$, the edges of each crystal were determined by stepping it in 1-μm steps through the beam and monitoring I_0.

Each crystal was then positioned so that the beam passed through its geometric center. The diffractometer coordinates of ω and χ were adjusted to optimize the intensity of the $(0,0,l)$ diffraction spectra. The detector was set at a 2θ angle of 15.000° for measurements on crystal A and at 13.000° for crystal B. These angular positions were calibrated using the diffraction pattern from an Au foil. When aligned, the diffracted intensity from the lower-energy peaks of the YBCO crystals was so intense that the Ge detector would saturate. To avoid this, an Al plate approximately 10 mm thick was placed in the incident beam to absorb lower-energy photons. A schematic of the experimental set up is shown in Fig. 8. The diffraction spectra from crystals A and B are shown in Figs. 9(a) and 9(b), respectively.

The length of the c axis can be determined from any $(0,0,l)$ peak. Since the (0,0,16) peak is the strongest in the measured spectrum for crystal A, only it was monitored. It also was selected because it is at a sufficiently high photon energy, 65.24 keV. For crystal B (at $2\theta = 13.000°$) the (0,0,11) peak at 51.47 keV was used for the same reasons. At these photon energies, the absorption length is sufficiently large to allow collection of data from anywhere in the crystal. The apertures in front of the energy-dispersive detector could not be reduced below about 20 μm; consequently, the measured spectra were collected from the horizontal length of the crystal illuminated by the incident beam. As the y position of the crystals is changed, the effective scattering center will undergo a small displacement due to absorption. The largest effect of this on the value of $(7-\delta)$ is calculated to be less than 0.3%.

The intensity around the selected diffraction peak, $E_{0,0,16}$ for crystal A and $E_{0,0,11}$ for crystal B, was measured as the crystal was systematically stepped through a series of (y,z) positions. This was accomplished automatically by a computer program ZSTP. The operations executed by ZSTP are as follows: (1) The crystal is translated to a new (y,z) position; (2) the diffraction peak of interest is centered in ω and χ; (3) the crystal is stepped in ω through the diffraction peak, and at each step, the number of counts in an energy window centered on the peak of interest and extending into the background on either side is recorded for a fixed time period; (4) the crystal is then translated to a new (y,z) position and the procedure repeated.

Three separate scans were made of each crystal. Values for and definitions of each of the input parameters for ZSTP were as follows:

Crystal A:

	Scan 1	Scan 2	Scan 3
y_0, Δy, $\#y=$	−0.20, 0.02, 12	−0.20, 0.02, 12	−0.20, 0.02, 12
z_0, Δz, $\#z=$	−0.05, 0.10, 16	−0.50, 0.10, 20	−0.40, 0.05, 34
$\#\omega$, $\Delta\omega$, $\Delta t:=$	7, 0.10, 7	7, 0.10, 11	7, 0.10, 10
ω_0, χ_0, $E_0=$	7.7, −2.5, 65.24	7.39, 1.7, 65.24	7.34, −2.37, 65.24
Center (ω,χ)?:	Yes	Yes	Yes
$\Delta\omega$, $\Delta\chi=$	0.05, 1.00	0.05, 0.50	0.05, 0.75

Crystal B:

	Scan 1	Scan 2	Scan 3
y_0, Δy, $\#y=$	−0.20, 0.05, 7	−0.20, 0.05, 7	−0.20, 0.05, 7
z_0, Δz, $\#z=$	−1.60, 0.10, 28	−1.60, 0.04, 7	−1.60, 0.05, 56
$\#\omega$, $\Delta\omega$, $\Delta t:=$	5, 0.05, 7	7, 0.05, 10	6, 0.02, 7
ω_0, χ_0, $E_0=$	9.265, 1.7, 51.47	9.265, 1.7, 51.47	9.265, 1.7, 51.47
Center (ω,χ)?:	Yes	Yes	Yes
$\Delta\omega$, $\Delta\chi=$	0.02, 0.50	0.02, 0.50	0.02, 0.50

where y_0, Δy, and $\#y$ are the initial y coordinate, the increment in y, and the number of steps in y, respectively; z_0, Δz, and $\#z$ are the same for z; $\#\omega$, $\Delta\omega$, and Δt are the number of ω positions at which the peak is to be measured, the increment between ω steps, and the duration (in seconds) for which the spectrum is to be measured, respectively; if the peak is to be recentered in ω and χ at each new (y,z) position, then $\Delta\omega$ and $\Delta\chi$ are the step increments in the centering procedure. All linear values are in mm, and all angular values are in degrees. The approximate duration for each of the three scans was 9, 12, and 17 h for crystal A and 7, 2, and 12 h for crystal B. In both cases, scan 3 was stopped before completion.

2. Data analysis

The output files from ZSTP were analyzed by separate program YZSCAN. The operations executed by YZSCAN are as follows: (1) Read the output file from ZSTP, (2) for each setting in y, z, and ω, determine if there is a peak present within the designated energy window; (3) if so, fit the data to a mathematical function; (4) find the center of the largest peak for all the ω settings at this (y,z) position; (5) output the results for graphical analyses.

The relative standard deviation in the net intensity (above background), σ, is given by the equation[74]

$$\sigma \equiv \frac{[N_t + N_b]^{1/2}}{N_t - N_b}, \tag{2}$$

where N_t is the total number of counts in the energy window and N_b is the total number of background counts. For crystal A, the energy window was 61 channels wide; for crystal B, it was 41 channels wide. The background is determined by a linear fit to the counts in the first and last five channels. For a peak to be recognized, σ needs to be less than a preset maximum, usually 0.1.

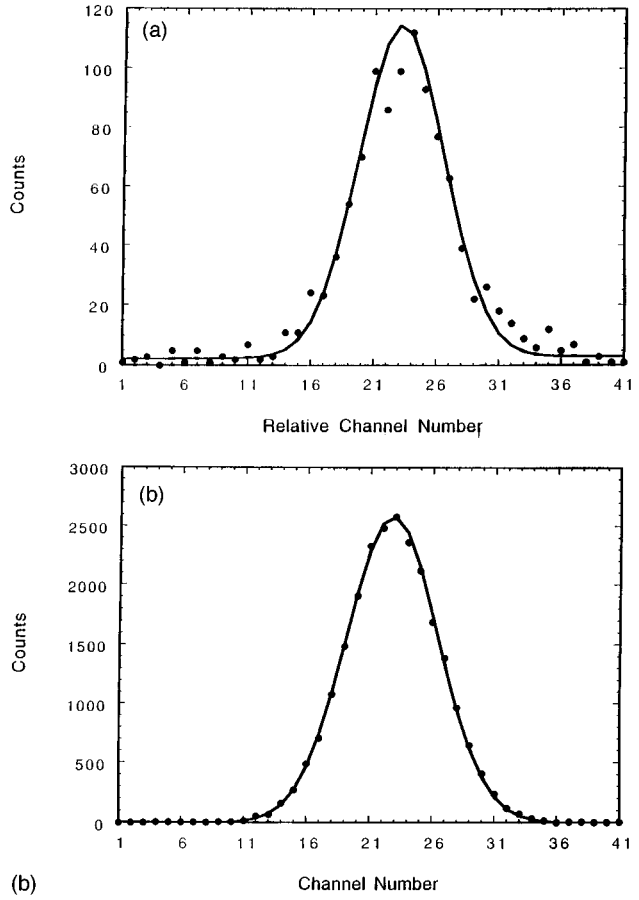

FIG. 10. (a) χ^2-sums fit to a weak peak. (b) χ^2-sums fit to a strong peak.

If a peak is determined to exist, then the data recorded in the energy window are fitted to a Gaussian function plus a linear background. The equation used to represent the data is

$$I_{\text{fit}}(n)=a_1\ \exp\left\{-\frac{1}{2}\left[\frac{(n-a_2)}{a_3}\right]^2\right\}+[a_4+a_5 n], \qquad (3)$$

where $I_{\text{fit}}(n)$ represents the number of counts in channel n and a_i $(i=1,2,\ldots,5)$ are the coefficients determined by the fit. The peak amplitude, center, and width are a_1, a_2, and a_3, respectively; the intercept and slope of the linear background function are a_4 and a_5, respectively. The values for a_i were evaluated by minimization of the goodness of the fit, χ^2:

$$\chi^2=\sum\left[\frac{1}{\sigma_n^2}\left[I_{\text{fit}}(n)-I_{\text{meas}}(n)\right]^2\right], \qquad (4)$$

where σ_n are the uncertainties in the data points, taken to be unity, and $I_{\text{meas}}(n)$ are the measured values of the intensity for each channel, n. A parabolic expansion of the χ^2 method was used for the determination of the a_i.[75] Iteration of the fitting routine was continued until the difference between subsequent χ^2 sums was less that a preset minimum, usually 0.001%. Typical fitted functions for a weak peak and for a strong peak are shown in Figs. 10(a) and 10(b), respectively.

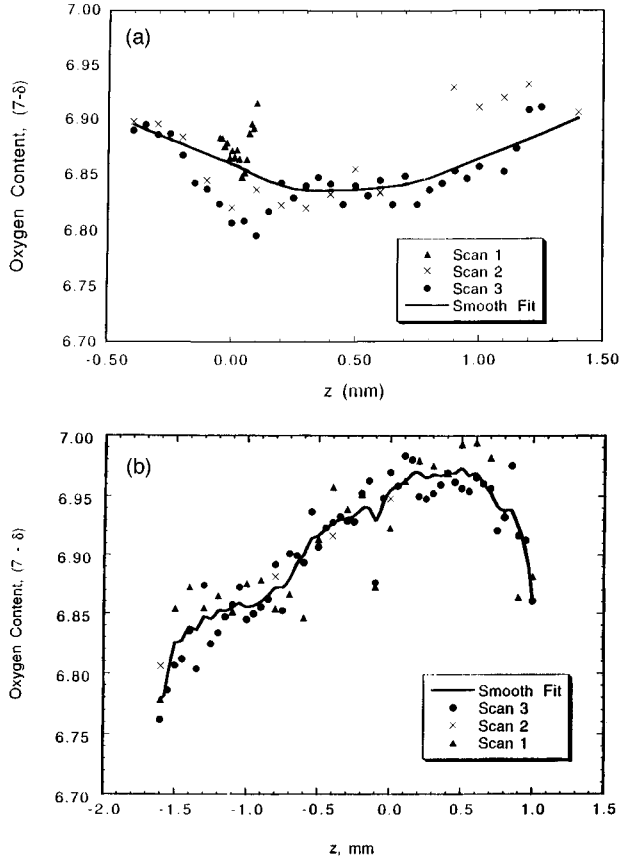

FIG. 11. (a) Values of $(7-\delta)$ vs z at $y=-0.06$ mm for scans 1, 2, and 3 for crystal A. (b) Values of $(7-\delta)$ vs z at $y=-0.05$ mm for scans 1, 2, and 3 for crystal B.

The peak channel number associated with a peak is converted into photon energy using a calibration curve for the detector determined using a series of known radioactive sources. The energy values are converted into c-axis lattice parameters using the Bragg relation

$$d_{hkl}=\frac{\kappa l}{2E_{hkl}\ \sin\ \theta}, \qquad (5)$$

where d_{hkl} is the interplanar spacing of the (h,k,l) planes, κ is the product of Planck's constant and the speed of light, E_{hkl} is the energy of the (h,k,l) diffraction peak, and 2θ is the Bragg angle. The c-axis length is equal to the product of l and d_{00l}. The previously cited linear relationship between the length of the c axis and $(7-\delta)$ was used to convert the data into oxygen content.

Finally, for each value of y and for each of the three scans for each crystal, the values of $(7-\delta)$ are plotted versus z. The plots for $y=-0.06$ for crystal A and $y=-0.05$ for crystal B are shown in Figs. 11(a) and 11(b), respectively, as representative examples. For each value of y, a smooth curve was then drawn through all three data sets. These smooth curves were used to generate the three-dimensional plots shown in Figs. 12(a) and 12(b) for crystals A and B, respectively. As with the surface measurements, no region of the crystal was observed to have a value of $(7-\delta)>7.0$, with the experimental uncertainty.

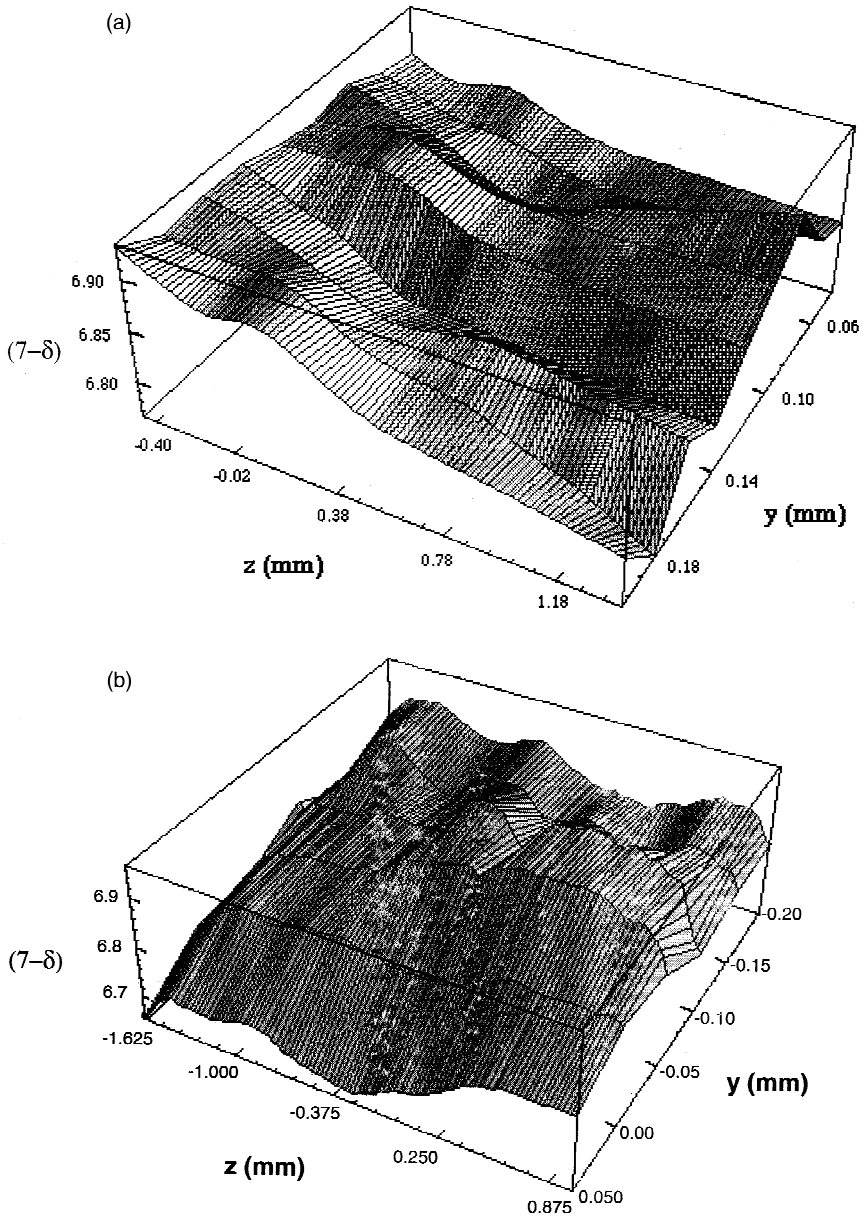

FIG. 12. (a) Three-dimensional plot of $(7-\delta)$ vs y and z for crystal A. (b) Three-dimensional plot of $(7-\delta)$ vs y and z for crystal B.

IV. CONCLUSION

Earlier studies of structural inhomogeneities in a number of YBCO crystals have shown that variations in $(7-\delta)$ are common. However, most of those crystals also had broad and/or multiple superconducting transitions, as would be expected. A summary of our results for samples A and B and other similar samples is shown in comparison to previously published results obtained by other groups in Table II. The results reported here demonstrate that even crystals with sharp transitions and low resistivities can possess numerous structural imperfections, implying that transport measurements alone are not a rigorous test of HTS sample quality. The consistency between our observations of transport properties in samples with known inhomogeneities and those obtained in samples that were assumed to be clean and homogeneous leads us to question whether any of the observed transport properties of the HTS's can be attributed solely to intrinsic behavior. We feel that these results present an opportunity for theorists to either explain why one can ignore sample imperfections or to predict how experimental results are affected by them.

We emphasize that the results presented here do not in any way provide evidence that sample inhomogeneities manifest themselves in the transport properties. However, the presence of such defects in two crystals which would otherwise be considered high quality based upon transport measurements alone makes it vital that any crystal which produces exotic experimental results be carefully examined to assay its defects. Until the transport properties are measured in a crystal whose oxygen content and homogeneity have been determined to be optimal via structural studies, the intrinsic nature of these materials remains uncertain. In addi-

TABLE II. Comparison of transport data obtained from various single-crystal samples of $YBa_2Cu_3O_{7-\delta}$ from this study with those obtained from the literature. The crystals from this study were shown via x-ray-diffraction measurements to contain oxygen defects.

Transport property	This study	Literature results
Low resistivity ρ (100 K)	40–60 $\mu\Omega$ cm	20–100 $\mu\Omega$ cm
High T_c	$\cong$93 K	92–95 K
Sharp ΔT_c	100–300 mK	100–300 mK
$\cot(\theta_H)=aT^2+b$	$a\cong 0.006$ K^2 b$\cong$10	$A\cong 0.005$ K^{-2} C$\cong$10–20
Negative ρ_{xy}	$\rho_{xy}(\text{min})=-0.4$ $\mu\Omega$ cm	ρ_{xy}(min) between -0.5 and -0.1 $\mu\Omega$ cm
Vortex lattice ''melting'' transition	Observed in twinned samples	Observed in twinned and untwinned samples
$7-\delta$	6.8–6.9	?

tion, since conventional x-ray-diffraction measurements do not achieve the resolution needed to measure the inhomogeneities reported in this study, only high-resolution x-ray-diffraction or other techniques which obtain similar resolution are appropriate for structural studies in the HTS systems.

ACKNOWLEDGMENTS

The authors gratefully acknowledge Dr. Terrell Vanderah of NIST for providing samples as well as Dr. S. A. Wolf and Dr. R. J. Soulen, Jr. of NRL for useful discussions.

[1] J. A. Martindale, S. E. Barrett, C. A. Klug, K. E. O'Hara, S. M. DeSoto, C. P. Clichter, T. A. Friedmann, and D. M. Ginsburg, Phys. Rev. Lett. **68**, 702 (1992).

[2] M. Takigawa, J. L. Smith, and W. L. Hults, Phys. Rev. B **44**, 7764 (1991).

[3] J. A. Martindale, S. E. Barrett, K. E. O'Hara, C. P. Slichter, W. C. Lee, and D. M. Ginsburg, Phys. Rev. B **47**, 9155 (1993).

[4] W. N. Hardy, D. A. Bonn, D. C. Morgan, R. Liang, and K. Zhang, Phys. Rev. Lett. **70**, 3999 (1993).

[5] Z.-X. Shen, D. S. Dessau, B. O. Wells, D. M. King, W. E. Spicer, A. J. Arko, D. Marshall, L. W. Lombardo, A. Kapitulnik, P. Dickinson, S. Doniach, J. DiCarlo, T. Loeser, and C. H. Park, Phys. Rev. Lett. **70**, 1553 (1993).

[6] D. J. Van Harlingen, D. A. Wollman, D. M. Ginsberg, and A. J. Leggett, Physica C **235–240**, 122 (1994).

[7] D. A. Wollman, D. J. Van Harlingen, J. Giapintzakis, and D. M. Ginsberg, Phys. Rev. Lett. **74**, 797 (1995).

[8] C. C. Tsuei, J. R. Kirtley, C. C. Chi, L. S. Yu-Jahnes, A. Gupta, T. Shaw, J. Z. Sun, and M. B. Ketchen, Phys. Rev. Lett. **73**, 593 (1994).

[9] J. C. Phillips, Phys. Rev. B **46**, 8542 (1992); Physica C **221**, 327 (1994).

[10] V. Kresin and S. Wolf, in *Novel Superconductivity*, edited by S. Wolf and V. Kresin (Plenum, New York, 1987); Phys. Rev. B **41**, 4278 (1990); V. Z. Kresin, H. Morawitz, and S. A. Wolf, in *High Temperature Superconductivity*: *Physical Properties, Microscopic Theory, and Mechanisms*, edited by Josef Ashkenazi, Stewart E. Barnes, Fulin Zuo, Gary C. Vezzoli, and Barry M. Klein (Plenum, New York, 1991).

[11] J. Mesot, P. Allenspach, U. Staub, A. Furrer, and H. Mutka, Phys. Rev. Lett. **70**, 865 (1993).

[12] M. S. Osofsky, J. L. Cohn, E. F. Skelton, M. M. Miller, R. J. Soulen, Jr., S. A. Wolf, and T. A. Vanderah, Phys. Rev. B **45**, 4916 (1992).

[13] H. Kupfer, I. Apfelstadt, R. Flukiger, C. Keller, R. Meier-Hirmer, B. Runtsch, A. Turowski, U. Wiech, and T. Wolf, Cryogenics **29**, 268 (1989).

[14] M. Daeumling, J. M. Seuntjens, and D. C. Larbalestier, Nature (London) **346**, 332 (1990).

[15] E. C. Jones, D. K. Christen, J. R. Thompson, R. Feenstra, S. Zhu, D. H. Lowndes, J. M. Phillips, M. P. Siegal, and J. D. Budai, Phys. Rev. B **47**, 8986 (1993).

[16] J. Halbritter, Phys. Rev. B **48**, 9735 (1993).

[17] J. Halbritter, J. Appl. Phys. **68**, 6315 (1990).

[18] J. L. Vargas and D. C. Larbalestier, Appl. Phys. Lett. **60**, 1741 (1992).

[19] A. Gauzzi and D. Pavuna, Appl. Phys. Lett. **66**, 1836 (1995).

[20] T. A. Friedmann, M. W. Rabin, J. Giapintzakis, J. P. Rice, and D. M. Ginsberg, Phys. Rev. B **42**, 6217 (1990).

[21] U. Welp, S. Fleshler, W. K. Kwok, J. Downey, Y. Fang, G. W. Crabtree, and J. Z. Liu, Phys. Rev. B **42**, 10 189 (1990).

[22] S. B. Qadri, M. S. Osofsky, V. M. Browning, E. F. Skelton, and T. A. Vanderah, Appl. Phys. Lett. **68**, 2729 (1996).

[23] T. Ito, K. Takenaka, and S. Uchida, Phys. Rev. Lett. **70**, 3995 (1993).

[24] T. R. Chien, Z. Z. Wang, and N. P. Ong, Phys. Rev. Lett. **67**, 2088 (1991).

[25] A. Carrington, D. J. C. Walker, A. P. Mackenzie, and J. R. Cooper, Phys. Rev. B **48**, 13 051 (1993).

[26] J. P. Rice, J. Giapintzakis, D. M. Ginsberg, and J. M. Mochel, Phys. Rev. B **44**, 10 158 (1991).

[27] H. Safar *et al.*, Phys. Rev. Lett. **69**, 824 (1992).

[28] W. K. Kwok, S. Fleshler, U. Welp, V. M. Vinokur, J. Downey, G. W. Crabtree, and M. M. Miller, Phys. Rev. Lett. **69**, 3370 (1992).

[29] M. Charalambous, J. Chaussy, P. Lejay, and V. Vinokur, Phys. Rev. Lett. **71**, 436 (1993).
[30] W. K. Kwok, J. Fendrich, S. Fleshler, U. Welp, J. Downey, and G. W. Crabtree, Phys. Rev. Lett. **72**, 1092 (1994).
[31] Y. Iye, S. Nakamura, and T. Tamegai, Physica C **159**, 616 (1989); M. Galffy and E. Zirngiebl, Solid State Commun. **68**, 929 (1988).
[32] T. R. Chien, T. W. Jing, N. P. Ong, and Z. Z. Wang, Phys. Rev. Lett. **66**, 3075 (1991).
[33] S. J. Hagen, C. J. Lobb, R. L. Greene, M. G. Forrester, and J. H. Kang, Phys. Rev. B **41**, 11 630 (1990); S. J. Hagen *et al.*, *ibid.* **47**, 1064 (1993).
[34] J. P. Rice, N. Rigakis, D. M. Ginsberg, and J. M. Mochel, Phys. Rev. B **46**, 11 050 (1992).
[35] R. Hauff, V. Breit, H. Claus, D. Herrmann, A. Knierim, P. Schweiss, H. Wuhl, A. Erb, and G. Muller-Vogt, Physica C **235–240**, 1953 (1994).
[36] E. Janod, A. Junod, T. Graf, K.-Q. Wang, G. Triscone, and J. Muller, Physica C **216**, 129 (1993).
[37] R. J. Cava, B. Batlogg, C. H. Chen, E. A. Rietman, S. M. Zahurak, and D. J. Werder, Nature (London) **329**, 423 (1987).
[38] R. J. Cava, B. Batlogg, C. H. Chen, E. A. Rietman, S. M. Zahurak, and D. J. Werder, Phys. Rev. B **36**, 5719 (1987).
[39] J. D. Jorgensen, B. W. Veal, A. P. Paulikas, L. J. Nowicki, G. W. Crabtree, H. Claus, and W. K. Kwok, Phys. Rev. B **41**, 1863 (1990).
[40] R. Beyers, B. T. Ahn, G. Gorman, V. Y. Lee, S. S. P. Parkin, M. L. Ramirez, K. P. Roche, J. E. Vazquez, T. M. Gur, and R. A. Huggins, Nature (London) **340**, 619 (1989).
[41] T. Zeiske, R. Sonntag, D. Hohlwein, N. H. Andersen, and T. Wolf, Nature (London) **353**, 542 (1991).
[42] B. W. Veal, A. P. Paulikas, H. You, H. Shi, Y. Fang, and J. W. Downey, Phys. Rev. B **42**, 6305 (1990).
[43] D. J. Werder, C. H. Chen, R. J. Cava, and B. Batlogg, Phys. Rev. B **38**, 5130 (1988).
[44] R. J. Cava, A. W. Hewat, B. Batlogg, M. Marezio, K. M. Rabe, J. J. Krajewski, W. F. Peck, Jr., and L. W. Rupp, Jr., Physica C **165**, 419 (1990).
[45] J. D. Jorgensen, Shiyou PEI, P. Lightfoot, Hao SHI, A. P. Paulikas, and B. W. Veal, Physica C **167**, 571 (1990).
[46] A. Zibold, K. Widder, M. Merz, H. P. Geserich, A. Erb, G. Müller-Vogt, and J. Kircher, Physica C **235–240**, 1093 (1994).
[47] H. Claus, U. Gebhard, G. Linker, K. Röberg, S. Riedling, J. Franz, T. Ishida, A. Erb, G. Müller-Vogt, and H. Wühl, Physica C **200**, 271 (1992).
[48] C. Namgung, J. T. S. Irvine, and A. R. West, Physica C **168**, 346 (1990).
[49] M. E. Parks, A. Navrotsky, K. Mocala, E. Takayama-Muromachi, A. Jacobson, and P. K. Davies, J. Solid State Chem. **79**, 53 (1989).
[50] E. F. Skelton, A. R. Drews, M. S. Osofsky, S. B. Qadri, J. Z. Hu, T. A. Vanderah, J. L. Peng, and R. L. Greene, Science **263**, 1416 (1994).
[51] E. F. Skelton, S. B. Qadri, M. S. Osofsky, A. R. Drews, P. R. Broussard, J. Z. Hu, L. W. Finger, T. A. Vanderah, D. Kaiser, J. L. Peng, S. A. Anlage, R. L. Greene, and J. Giapintzakis, Proc. SPIE **2516**, 160 (1995).
[52] T. A. Vanderah, C. K. Lowe-Ma, D. E. Bliss, M. W. Decker, M. S. Osofsky, E. F. Skelton, and M. M. Miller, J. Cryst. Growth **118**, 385 (1992); M. S. Osofsky, J. L. Cohn, E. F. Skelton, M. M. Miller, R. J. Soulen, Jr., S. A. Wolf, and T. A. Vanderah, Phys. Rev. B **45**, 4916 (1992).
[53] U. Poppe, N. Klein, K. Dahne, H. Soltner, C. L. Jia, B. Kabius, K. Urban, A. Lubig, K. Schmidt, S. Hensen, S. Orbach, G. Muller, and H. Piel, J. Appl. Phys. **71**, 5572 (1992).
[54] T. R. Chien, Z. Z. Wang, and N. P. Ong, Phys. Rev. Lett. **67**, 2088 (1991).
[55] A. Carrington, D. J. C. Walker, A. P. Mackenzie, and J. R. Cooper, Phys. Rev. B **48**, 13 051 (1993).
[56] P. W. Anderson, Phys. Rev. Lett. **67**, 2092 (1991).
[57] A. Carrington, A. P. Mackenzie, C. T. Lin, and J. R. Cooper, Phys. Rev. Lett. **69**, 2855 (1992).
[58] T. Manako, Y. Kubo, and Y. Shimakawa, Phys. Rev. B **46**, 11 019 (1992).
[59] A. S. Alexandrov, A. M. Bratkovsky, and N. F. Mott, Phys. Rev. Lett. **71**, 1734 (1994).
[60] J. P. Rice, N. Rigakis, D. M. Ginsberg, and J. M. Mochel, Phys. Rev. B **46**, 11 050 (1992).
[61] J. Luo, T. P. Orlando, J. M. Graybeal, X. D. Wu, and R. Muenchausen, Phys. Rev. Lett. **68**, 690 (1992).
[62] J. Colino, M. A. Gonzalez, J. I. Martín, M. Velez, D. Oyola, P. Prieto, and J. L. Vicent, Phys. Rev. B **49**, 3496 (1994).
[63] J. M. Harris, N. P. Ong, and Y. F. Yan, Phys. Rev. Lett. **71**, 1242 (1993).
[64] Y. Iye, S. Nakamura, and T. Tamegai, Physica C **159**, 616 (1989).
[65] S. J. Hagen, C. J. Lobb, R. L. Greene, and M. Eddy, Phys. Rev. B **43**, 6246 (1991).
[66] Z. D. Wang and C. S. Ting, Phys. Rev. Lett. **67**, 3618 (1991).
[67] J. M. Harris, N. P. Ong, and Y. F. Yan, Phys. Rev. Lett. **73**, 610 (1994); J. M. Harris, N. P. Ong, P. Matl, R. Gagnon, L. Taillefer, T. Kimura, and K. Kitazawa, Phys. Rev. B **51**, 12 053 (1995).
[68] V. B. Geshkenbein and A. I. Larkin, Phys. Rev. Lett. **73**, 609 (1994).
[69] A. Dorsey, Phys. Rev. B **46**, 8376 (1992); N. B. Kopnin, B. I. Ivlev, and V. A. Kalatsky, J. Low Temp. Phys. **90**, 1 (1993).
[70] H. Safar, P. L. Gammel, D. A. Huse, and D. J. Bishop, Phys. Rev. Lett. **69**, 824 (1992).
[71] W. K. Kwok, S. Fleshler, U. Welp, V. M. Vinokur, J. Downey, G. W. Crabtree, and M. M. Miller, Phys. Rev. Lett. **69**, 3370 (1992).
[72] B. E. Warren, *X-Ray Diffraction* (Addison-Wesley, Reading, MA, 1969), pp. 328–329.
[73] E. F. Skelton, S. B. Qadri, M. S. Osofsky, A. R. Drews, P. R. Broussard, J. Z. Hu, L. W. Finger, T. A. Vanderah, D. Kaiser, J. L. Peng, S. A. Anlage, R. L. Greene, and J. Giapintzakis, Proc. SPIE **2516**, 160 (1995).
[74] H. P. Klug and L. E. Alexander, *X-Ray Diffraction Procedures* (Wiley, New York, 1954), p. 272.
[75] Philip R. Bevington, *Data Reduction and Error Analysis for the Physical Sciences* (McGraw-Hill, New York, 1969), pp. 222–231.